

SurvLatent ODE : A Neural ODE based time-to-event model with competing risks for longitudinal data improves cancer-associated Deep Vein Thrombosis (DVT) prediction

Intae Moon

*Electrical Engineering and Computer Science
Massachusetts Institute of Technology
Cambridge, MA, USA*

ITMOON@MIT.EDU

Stefan Groha

*Division of Population Sciences
Dana-Farber Cancer Institute
Boston, MA, USA*

STEFANM_GROHA@DFCI.HARVARD.EDU

Alexander Gusev

*Division of Population Sciences
Dana-Farber Cancer Institute
Boston, MA, USA*

ALEXANDER_GUSEV@DFCI.HARVARD.EDU

Abstract

Effective learning from electronic health records (EHR) data for prediction of clinical outcomes is often challenging because of features recorded at irregular timesteps and loss to follow-up as well as competing events such as death or disease progression. To that end, we propose a generative time-to-event model, SurvLatent ODE, which adopts an Ordinary Differential Equation-based Recurrent Neural Networks (ODE-RNN) as an encoder to effectively parameterize a latent representation under irregularly sampled data. Our model then utilizes the latent representation to flexibly estimate survival times for multiple competing events without specifying shapes of event-specific hazard function. We demonstrate competitive performance of our model on MIMIC-III, a freely-available longitudinal dataset collected from critical care units, on predicting hospital mortality as well as the data from the Dana-Farber Cancer Institute (DFCI) on predicting onset of Deep Vein Thrombosis (DVT), a life-threatening complication for patients with cancer, with death as a competing event. SurvLatent ODE outperforms the current clinical standard Khorana Risk scores for stratifying DVT risk groups.

1. Introduction

Electronic Health Records (EHR), which consist of longitudinal measurements of patients' measurements often extending over decades, offer unique opportunities to build data-driven clinical decision support tools. Accurate stratification of future disease can allow clinicians to focus clinical resources on the most at-risk patients while minimizing potential side effects and overtreatment for low-risk patients (Myers et al., 2017; Maniruzzaman et al., 2018; Zeiberg et al., 2019). However, most existing patient stratification tools still rely on simple, outcome-specific scoring systems that utilize a small number of static features. As patients

are often treated over the course of multiple interactions, a data-driven clinical decision model should relate the heterogeneous temporal evolution of clinical measurements to the clinical outcome in a flexible form and provide updated outcome prediction as a patient’s condition and clinical features change. As EHR data is typically collected incidentally, the model should appropriately handle data missingness due to irregular spacing of visits or loss to follow-up, as well as informative missingness – where the collection of a measurement may itself be predictive of a future outcome. When estimating risk of a clinical outcome, an effective clinical decision model should also consider potential competing events a patient may experience and update the risk for the outcome of interest accordingly. This enables clinicians to jointly consider the risk of cancer-specific death or a treatment-related toxicity when planning a therapeutic intervention.

One widely utilized risk prediction framework is a time-to-event (or survival) analysis, which models the lifetime of a patient until a failure event. Importantly, survival analysis can directly model outcomes that are lost to follow-up (also known as right-censoring), which is very common in EHR due to the lack of formal patient recruitment. One of the most widely utilized time-to-event models is the Cox proportional hazard model, a multivariable, semi-parametric framework proposed by [Cox \(1972\)](#), which relates log of relative hazard to a linear function of baseline features. Recently, there have been efforts to augment the Cox proportional hazard model by learning a non-linear relationship of baseline features to outcomes through deep neural networks ([Katzman et al., 2018](#); [Nagpal et al., 2021b](#)). However, these models make survival predictions based on a single snapshot of features and fail to capture evolution of time-varying features, often informative of predicting disease onset. To address this gap, time-to-event methods capable of handling time-varying, longitudinal measurements have been proposed. For example, some models utilized class of Recurrent Neural Network (RNN) models to learn input temporal representation which then renders estimated survival predictions ([Ren et al., 2018](#); [Lee et al., 2020](#); [Nagpal et al., 2021a](#)), while other models utilized a deep generative approach to model the event time distribution in a Bayesian framework ([Ranganath et al., 2016](#); [Miscouridou et al., 2018](#)). However, presented with potentially informatively missing measurements, these models rely on strategies agnostic to hidden time-dependent dynamics between observations and may lead to ill-defined latent representation.

In a multivariate time-series framework, many approaches have been developed to effectively handle informative missingness to improve prediction performance ([Choi et al., 2016](#); [Lipton et al., 2016](#); [Futoma et al., 2017](#); [Soleimani et al., 2017](#); [Che et al., 2018](#)). One approach to deal with missing values involves deploying a decay mechanism on both input data and RNN hidden states for describing dynamics under missing observations ([Che et al., 2018](#)). Other methods utilized a Gaussian process (GP)-based framework to learn dynamics across observed measurements and provide continuous latent states ([Futoma et al., 2017](#); [Soleimani et al., 2017](#)). However, these models rely on parametric assumptions on the latent dynamics, specified by either exponential decay functions or GP kernel functions with a stationary property and may not necessarily describe true latent dynamics. On the other hand, a recently proposed family of Neural Ordinary Differential Equations (Neural ODE) based models ([Chen et al., 2018](#); [Rubanova et al., 2019](#)) learns the latent dynamics using highly flexible neural network parameterized functions and is capable of handling input data

which may arrive at arbitrary time points, providing an avenue to model longitudinal data with missing values without strong parametric assumptions on the latent dynamics.

In this work, we present a generative, time-to-event model, SurvLatent ODE, which utilizes the Neural ODE framework to effectively learn temporal dynamics of the input representation under irregularly sampled measurements. Adopting a multi-task learning framework, our proposed model allows the underlying mechanism of multiple events to be shared in the latent representation while utilizing a cause-specific decoder module to flexibly learn signals specific to each event from the shared latent representation. As a result, the proposed model provides survival functions for each patient across multiple clinical outcomes they may encounter while incorporating temporal evolution of their covariates. Using MIMIC-III, a publicly available longitudinal dataset which consists of patients' covariates at critical care units, we demonstrate that the proposed model significantly outperforms conventional as well as state-of-the-art survival models in predicting time to hospital mortality. Furthermore, we utilize the longitudinal data from the Dana-Farber Cancer Institute (DFCI) for predicting time to DVT with all-cause mortality as a competing event, and show that the proposed model significantly outperforms the current clinical standard, Khorana scores (Khorana et al., 2008). Finally, we show the learned latent representation offers interpretable clusters of patients with meaningfully different outcomes. The implementation of SurvLatent ODE model is available at https://github.com/itmoon7/survllatent_ode.

Generalizable Insights about Machine Learning in the Context of Healthcare

- To the best of our knowledge, our proposed model is the first demonstration of the ODE-based variational autoencoder time-to-event model for longitudinal data where temporal latent dynamics in the input data are explicitly modeled via neural networks.
- Combined with the effective longitudinal modeling, our proposed framework enables flexible non-parametric estimation of hazard functions for the event of interest as well as competing events via a multi-task learning framework, which gains significant improvements over conventional and recently published deep learning based survival models.
- Applied to the in-house dataset of Deep Vein Thrombosis (DVT) events, our model significantly outperforms current clinical standards, Khorana scores (Khorana et al., 2008) and provides insights into influential features for elevated DVT risks via interpretable latent representations.

2. Related Work

Deep learning based approaches have been widely utilized in many published work in the context of time-to-event analysis to learn complex, non-linear relationship between covariates via neural networks (Lee et al., 2018a; Katzman et al., 2018; Nagpal et al., 2021b), Convolutional Neural Network (CNN) (Jarrett et al., 2018), Gaussian Process (Alaa and van der Schaar, 2017), and Recurrent Neural Networks (Ren et al., 2018). However, all of the above models only consider patients' time static features at baseline. More recently, several methods have been developed to incorporate time-varying features. Recurrent

Deep Survival Machines (Nagpal et al., 2021a) incorporates time-varying features from longitudinal data and estimates conditional survival distribution through a fixed mixture of parametric distributions like Weibull or Log-Normal. However, a parametric assumption on the underlying time-to-event process may lead to a model miss-specification and limit the flexibility of relating neural network-learned representations to the conditional survival estimates. Furthermore, the model only handles a single risk, which may lead to an overestimation of the disease risk since in healthcare applications there is often a varying degree of dependence across competing events (Berry et al., 2010; Austin et al., 2016). Lee et al. (2020) proposed Dynamic-Deephit, a non-parametric, discrete time-to-event model, which incorporates time-varying features and utilizes a multi-task learning framework to estimate joint distribution of the first hitting time and competing events. A key assumption of the model is that a patient experiences an event over the predefined finite time horizon with a probability of 1, which often does not hold in real data. Both models rely on a model agnostic imputation strategy which utilizes population-level statistics (e.g. means) and/or missing data indicators (Lipton et al., 2016). Ranganath et al. (2016) and Mscouridou et al. (2018) demonstrated survival models where missing observations were handled by a shared latent process which models observed measurements as well as event times in a Bayesian framework. However, their models relied on strong exponential parametric assumption on the underlying data generating process and were not evaluated in the longitudinal setting.

In the context of more conventional survival statistical models for competing risks, cause-specific Cox regression and Fine-Gray Cox regression (Fine and Gray, 1999) models are widely used for the analysis of continuous event times. These two models have been extended to the analysis involving event times measured on a discrete time scale (Lee et al., 2018b; Berger et al., 2020). While the Fine-Gray model enables estimation of covariates' effects on the cumulative incidence function for the event of interest, the cause-specific Cox model captures effect of covariates on the cause-specific hazard function for each event, which denotes the instantaneous rate of the corresponding event occurrence for patients who are currently event free (Putter et al., 2007; Austin et al., 2016). Both models assume linear relationship between patients' covariates and log of the relative hazard as well as proportional hazard where effects of covariates on the relative hazards remain constant over time. However, these assumptions are limiting because true underlying time-to-event processes are often described by complex nonlinear relationships between patients' biomarkers and effects of biomarkers on the survival may change over time as patients' health status are changing.

Ordinary Differential equations parameterized by neural networks, popularized by Chen et al. (2018), have been utilized in time-to-event analysis in a multi-state setting (Groha et al., 2021) and a single-event continuous-time setting (Tang et al., 2020). Groha et al. (2021) proposes a Neural ODE approach to estimate the Kolmogorov forward equations which then provides transition probabilities in a multi-state framework. Tang et al. (2020) models the distribution of survival time for a single event by learning the dynamics of the cumulative hazard function via Neural ODE. However, both approaches only considered the baseline data and left out informative signals from time-varying covariates. To the best of our knowledge, our proposed model is the first demonstration of full ODE-based encoder-decoder architecture for modeling longitudinal data in a time-to-event framework.

3. Methods

3.1. Preliminaries

We first introduce three key modeling choices of the proposed framework : Neural Ordinary Differential Equations (Neural ODEs), discrete survival analysis, and competing risks.

3.1.1. NEURAL ORDINARY DIFFERENTIAL EQUATIONS

First, we model a patient’s health trajectory using Neural Ordinary Differential Equations (Neural ODEs). Neural ODEs are a recently proposed family of neural networks-based continuous time models (Chen et al., 2018), which parameterize the dynamics of a hidden state $h(t)$. This hidden state can be the latent health trajectory of a patient and a function of their time-varying covariates (i.e. $h(t) = z_1(X^t)$, where $z_1(\cdot)$ may be neural networks and X^t is a set of patient’s covariates up until time t). Given that the function f_θ (parameterized by the neural network) specifies the dynamics of the hidden state, we can define the hidden state $h(t)$ (e.g. a latent health trajectory) at any arbitrary time t as follows:

$$h(t) = h(t_0) + \int_{t_0}^t f_\theta(h(\tau), \tau) d\tau, \quad (1)$$

where $h(t_0)$ is an initial hidden state. Rubanova et al. (2019) demonstrated that this Neural ODE framework can be incorporated into a Recurrent Neural Network (RNN) model, allowing f_θ to learn the dynamics of the RNN hidden state $h(t)$ such that $h(t)$ is well-defined in a continuous time. Such an ODE-RNN model can incorporate irregularly sampled input data without having to explicitly impute missing values. Finally, the hidden state trajectory may be further decoded into, for example, the hazard function trajectory, $\lambda(t)$ for a time-to-event analysis.

3.1.2. DISCRETE SURVIVAL ANALYSIS

Second, we model the outcome event times as a discrete time process. A common constraint of healthcare data is that event times such as time of hospital death and time of stroke diagnosis are often recorded on a discrete time scale, for example, in hours or days. In this case, the exact time of an event is not known and all we know is that the event occurred between two consecutive time points. Formally, a continuous time horizon is divided into discrete intervals (i.e. $[0, t_1], [t_1, t_2], \dots$), where time resolution is often determined by a domain knowledge, and event time denoted by $T = t$ means that the event of interest has happened in the interval $[t - 1, t)$ (Tutz and Schmid, 2016).

3.1.3. COMPETING RISKS

Third, we seek to model multiple competing outcomes (e.g. cancer-specific death, metastasis, and DVT) that a patient is under risk for simultaneously. One common approach to handle competing risks in a discrete survival analysis is to model the cause-specific discrete hazard function (i.e. rate of the event occurrence in a current time interval for event free patients in the previous time interval) (Austin et al., 2016). At a patient level, this framework provides insights on the individual event mechanism by modeling the contribution of a patient’s

covariates on the hazard function over time. Formally, given K different competing events and a set of covariates X , the cause-specific discrete hazard function $\lambda_k(t)$ for event k is

$$\lambda_k(t|X) = P(T = t, K = k|T \geq t, X). \quad (2)$$

And the resulting overall discrete hazard function is

$$\lambda(t|X) = \sum_{k=1}^K \lambda_k(t|X) = P(T = t|T \geq t, X). \quad (3)$$

An overall event-free survival probability $S(t|X)$ is

$$S(t|X) = P(T > t|X) = \prod_{\tau \leq t} (1 - \lambda(\tau|X)). \quad (4)$$

Finally, the cause-specific cumulative incidence function (CIF) for event k , $F_k(t|X)$, which captures the risk for event k at time t under the other competing risks conditioned on X , is

$$F_k(t|X) = P(T \leq t, K = k|X) = \sum_{\tau}^t P(T = \tau, K = k|X) = \sum_{\tau}^t \lambda_k(\tau|X) S(\tau - 1|X). \quad (5)$$

3.2. Notation and setting

In brief, our model takes as input a set of individuals with (possibly irregularly spaced) time-varying covariates and event times of one or more outcome events, and learns the functions that map the covariates to each outcome specific hazard over time. We formalize these variables below.

The survival dataset \mathcal{D} with sample size N is a set of tuples $\{(t_i, k_i, \mathcal{X}_i)\}_{i=1}^N$ where t_i and k_i are the observed survival time and the event type for sample i , respectively. Note that $t_i = \min(\tilde{T}_i, C_i)$ where \tilde{T}_i is the true event time and C_i is the right censoring (i.e. loss to follow-up) time of sample i . Therefore, for right-censored samples (i.e. those with $\tilde{T}_i > C_i$), t_i corresponds to C_i .

In the competing risks scenario, there may be multiple events where an occurrence of one of those events prevents the occurrence of the other events (for example, illness cannot occur after death). To that end, given the finite set of K mutually exclusive competing events, $\mathcal{K} = \{0, 1, \dots, K\}$, the event type of sample i is denoted by $k_i \in \mathcal{K}$, where $k_i = 0$ corresponds to the right-censoring of sample i . Note that throughout this paper, we assume that the censoring mechanism is non-informative.

\mathcal{X}_i is the set of covariates for sample i longitudinally measured at some irregular timestamps denoted by τ_i . In other words, given that $\tau_{i,0}$ and $\tau_{i,l}$ are the initial measurement time and latest measurement time for sample i , respectively, $\mathcal{X}_i = \{x_i(\tau_{i,0}), x_i(\tau_{i,1}), \dots, x_i(\tau_{i,l})\}$, where $x_i(\tau_i) \in \mathbb{R}^M$ and M is the number of covariates. Let T_i^r be a random variable for the remaining time-to-event from the latest measurement $\tau_{i,l}$ for sample i . Our goal is to estimate the discrete cause-specific hazard function denoted by $\lambda_k(t|\mathcal{X}_i, Z_i^t) = P(T_i^r = t, k_i = k|T_i^r \geq t, \mathcal{X}_i, Z_i^t)$, where Z_i^t is the latent trajectory representing the data \mathcal{X}_i up until time t . For the rest of our paper, we use $\lambda_{i,k}^*(t)$ to denote $\lambda_k(t|\mathcal{X}_i, Z_i^t)$. Finally, we can relate $\lambda_{i,k}^*(t)$ to the overall event-free survival function, $S(t|\mathcal{X}_i)$, as well as cause-specific CIF, $F_k(t|\mathcal{X}_i)$, to assess individual risk of experiencing event k .

3.3. SurvLatent ODE

3.3.1. OVERVIEW OF THE MODEL ARCHITECTURE

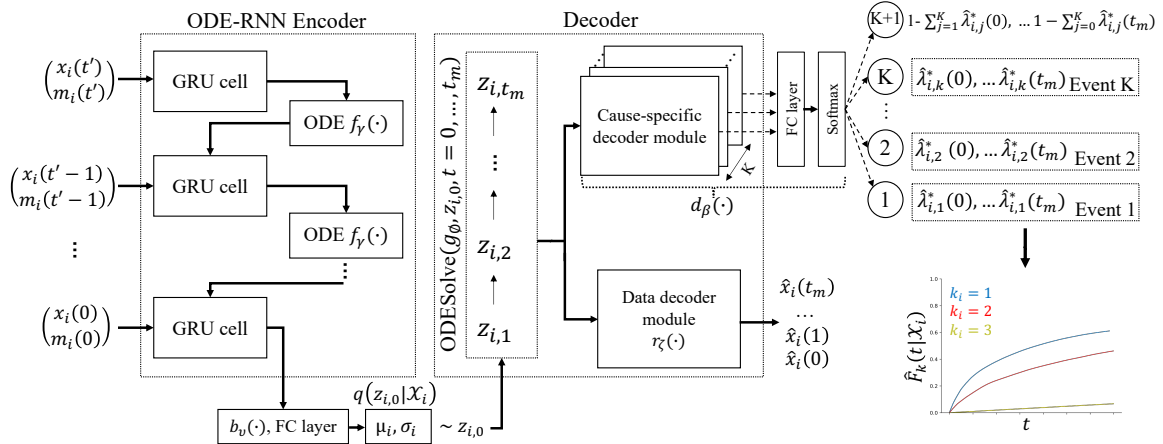


Figure 1: **Model architecture of SurvLatent ODE** : the ODE-RNN encoder parametrizes a patient-specific temporal trajectory of covariates $x_i(0), \dots, x_i(t')$ into the latent embedding and describes approximate posterior over the initial latent variable $z_{i,0}$. The sampled initial latent variable $z_{i,0}$ is then decoded into the latent trajectory, $Z_i^{t_m} = (z_{i,0}, z_{i,1}, \dots, z_{i,t_m})$ by calling a black-box differential equation solver $\text{ODESolve}(g_\phi, z_{i,0}, t = 0, \dots, t_m)$. Finally, $d_\beta(\cdot)$, which consists of cause-specific decoder modules, subsequent fully connected layer, and softmax layer, maps the corresponding latent trajectory to estimate cause-specific hazard function for each event.

The overall architecture of SurvLatent ODE is shown in Fig. 1. Following the recently proposed latent-variable time series model (Chen et al., 2018; Rubanova et al., 2019), we adopt a generative, variational autoencoder framework (Kingma and Welling, 2013) to model time-varying covariates. In a high level, a patient-specific temporal trajectory of covariates with a varying time length, denoted by \mathcal{X}_i is encoded into the latent embedding with a fixed dimension via the ODE-RNN encoder. The patient specific embedding is then decoded into the latent trajectory with pre-specified length t_m (i.e. $Z_i^{t_m} = (z_{i,0}, z_{i,1}, \dots, z_{i,t_m})$) by evaluating the integral with $g_\phi(\cdot)$ as the integrand, where $g_\phi(\cdot)$ is parameterized by the neural networks and describes the latent dynamics. Finally, we utilized cause-specific decoder modules, which consists of fully connected neural networks, to estimate hazard function for each event over time.

On the encoder side, in order to learn the latent dynamics of the input temporal data and parameterize approximate posterior over z_0 (i.e. $q(z_0 | \mathcal{X})$), we utilize a ODE-RNN (Rubanova et al., 2019) as an encoder. A function $f_\gamma(\cdot)$, parameterized by neural networks with γ as trainable weights, specifies the dynamics of RNN hidden states, which allows the RNN to have continuously well-defined hidden states and incorporate inputs arriving at arbitrary times. This is the key element in the ODE-RNN encoder, which makes it unnecessary to explicitly impute missing measurements. When feeding the data into the model, we zero-fill missing measurements and concatenate the vector of indicators for missing measurements, $m(t)$, into the input data at time t , $x(t)$. The hidden states are updated at time points when measurements are available.

For a RNN model, we utilize a Gated Recurrent Unit (GRU) cell (Cho et al., 2014), which resolves the vanishing or exploding gradient problems of conventional RNNs and enables learning long-term temporal dependencies across the data. Given the set of longitudinal data \mathcal{X} with the latest measurement time of t' , the ODE-RNN encoder runs backwards in time from t' to 0 to get the approximate posterior $q(z_0|\mathcal{X})$ as follows:

$$\begin{aligned} q(z_0|\mathcal{X}) &= \mathcal{N}(\mu_{z_0}, \sigma_{z_0}) \\ \mu_{z_0}, \sigma_{z_0} &= b_v(\text{ODE-RNN}_{\theta, f_\gamma(\cdot)}(\mathcal{X})), \end{aligned} \quad (6)$$

where θ corresponds to a set of trainable weights in the GRU cell and b_v is a neural network with weights v and relates the final hidden state of the ODE-RNN encoder to the mean and variance over z_0 . As a result of the ODE-RNN encoder, temporal latent dynamics of the hidden states are flexibly modeled by neural networks without resorting to any strong parametric assumptions on the dynamics (Rubanova et al., 2019).

On the decoder side, we utilize a multi-tasking learning framework (Caruana, 1997; Alaa and van der Schaar, 2017; Lee et al., 2020) and allow for the latent trajectory Z^t to be shared across multiple events. For patient i , the latent trajectory Z_i^t is obtained by sampling the initial state $z_{i,0}$ from the approximate posterior $q(z_{i,0})$ and evaluating the integral, $z_{i,0} + \int_0^t g_\phi(z_{i,u}, u) du$ at pre-specified time points (i.e. $t = 0, \dots, t_m$, where t_m is the end time point of the prediction window and may be arbitrarily far into the future). This integral can be computed by calling a black-box differential equation solver, ODESolve($g_\phi, z_{i,0}, t = 0, \dots, t_m$) (Chen et al., 2018). Then, each cause-specific decoder module out of total K modules learns a flexible event-specific function which maps the latent trajectory Z^t shared across K events to the cause-specific hazard function for each event $\lambda_k(t)$ (see Section 3.3.2). This operationalizes the intuition that multiple clinical outcomes can have partially shared latent mechanisms. For example, the clinical outcomes such as DVT, cancer-specific death, and metastasis can have a shared latent mechanism driven by types of malignant tumors and blood protein tests. Finally, the data decoder module reconstructs a patient-specific data trajectory across the pre-specified time window (i.e. $\hat{x}_i(0), \hat{x}_i(1), \dots, \hat{x}_i(t_m)$), which could potentially be used for interpolation and extrapolation tasks.

3.3.2. SURVIVAL FUNCTION ESTIMATION

Survival function estimation in our model comes down to learning the function, $d_\beta(\cdot)$, which maps the sampled patient-specific latent trajectory, $Z_i^{t_m}$ to the cause-specific hazard function for event k , $\lambda_{i,k}^*(t)$ evaluated across the pre-specified time window $[0, t_m]$. Then, we utilize the hazard function to estimate event free survival probability as well as cause-specific cumulative incidence function over the appropriate time window. β corresponds to a set of trainable weights in cause-specific decoder modules and the subsequent fully-connected layer as shown in Fig. 1. Recall that in our discrete survival analysis framework, $\lambda_{i,k}^*(t) = P(T_i^r = t, K = k | T_i^r \geq t, \mathcal{X}_i, Z_i^t)$ where the hazard remains fixed in each time; bin widths are specified based on domain knowledge (e.g. a day or an hour). Note that our model does not specify any functional forms for how the data \mathcal{X} relate to the $\lambda_k^*(t)$ and allow the neural networks to flexibly parameterize hazard functions. With the assumption that data (\mathcal{X}) is independent of remaining time-to-event (T^r) conditioning on the sampled latent

state (Z^t), the event free survival survival probability $S(t|\mathcal{X}_i, Z_i^t)$ for patient i is estimated using the corresponding latent trajectory Z_i^t (i.e. patient i 's latent trajectory up until t) as follows:

$$\hat{S}(t|\mathcal{X}_i, Z_i^t) = \hat{S}(t|Z_i^t) = \hat{P}(T_i^r > t|Z_i^t) = \prod_{\tau_{i,l} < \tau \leq t} \left(1 - \sum_{k=1}^K \hat{\lambda}_{i,k}^*(\tau) \right), \quad (7)$$

where $\tau_{i,l}$ is the latest measurement time for the patient. Setting a lower-bound for τ with $\tau_{i,l}$ is necessary since $S(t|Z_i^t)$ should always be 1 for $t \in [0, \tau_{i,l}]$. The proof for Equation 7 is shown in Appendix A. Notice that at any given time point τ , $\sum_{k=0}^K \lambda_{i,k}^*(\tau)$ must sum up to 1, where $\lambda_{i,0}^*(\tau) = 1 - \sum_{k=1}^K \lambda_{i,k}^*(\tau)$ and denotes probability of not experiencing any events at time τ given patient i survives up to the prior time point (i.e. $\tau - 1$). We enforce this constraint using the softmax layer as shown in Fig. 1. Finally, the estimated cause-specific cumulative incidence function $\hat{F}_k(t|Z_i^t)$ is

$$\hat{F}_k(t|Z_i^t) = \hat{P}(T \leq t, K = k|Z_i^t) = \sum_{\tau_{i,l} < \tau \leq t} \hat{P}(T = \tau, K = k|Z_i^t) = \sum_{\tau_{i,l} < \tau \leq t} \hat{\lambda}_{i,k}^*(\tau) \hat{S}(\tau - 1|Z_i^t). \quad (8)$$

3.4. Inference

We devise the loss function which handles time-varying covariates as well as loss to follow-up (i.e. right-censoring). The total loss consists of two components : the Kullback-Leibler (KL) divergence loss (i.e. $D_{KL}[q(z_0|\mathcal{X}) \parallel p(z_0|\mathcal{X})]$), where $q(z_0)$ is the approximate posterior over the initial latent state and \mathcal{X} is the set of time-varying covariates, and the log of the total survival likelihood. In practice, the KL loss cannot be directly evaluated since the posterior distribution $p(z_0|\mathcal{X})$ is intractable because computing evidence $p(\mathcal{X})$ involves marginalizing out high-dimensional latent variable z_0 . Therefore, we instead maximize the evidence lower bound (ELBO) :

$$\text{ELBO}(\mathcal{X}; \Phi, \zeta) = \mathbb{E}_{q(z_0|\mathcal{X}; \Phi)}[\log(p(\mathcal{X}|z_0; \phi, \zeta))] - \text{KL}[q(z_0|\mathcal{X}; \Phi) \parallel p(z_0)], \quad (9)$$

where $p(z_0)$ is assumed to be a standard normal, Φ corresponds to a set of trainable weights $\{\theta, \gamma, v, \phi\}$ in the ODE-RNN encoder and $g_\phi(\cdot)$ which specifies dynamics of the latent trajectory on the decoder side, and ζ is a set of trainable weights in the data decoder module, $r_\zeta(\cdot)$. Maximizing the ELBO in this way is equivalent to minimizing the KL divergence (Bishop, 2006).

The total survival likelihood L_{surv} , which enables handling of right-censored patients, is estimated as follows:

$$\begin{aligned} L_{\text{surv}}(\mathcal{D}; \Phi, \beta) &= \prod_{i \in \mathcal{D}} \hat{P}(T_i^r = t_i^r, K = k_i; \Phi, \beta)^{\mathbb{1}\{k_i \neq 0\}} \times \hat{P}(T_i^r > t_i^r; \Phi, \beta)^{1 - \mathbb{1}\{k_i \neq 0\}} \\ &= \prod_{i \in \mathcal{D}} \left[\hat{\lambda}_{i,k}^*(t_i^r; \Phi, \beta) \hat{S}(t_i^r - 1|X_i; \Phi, \beta) \right]^{\mathbb{1}\{k_i \neq 0\}} \times \hat{S}(t_i^r|X_i; \Phi, \beta)^{1 - \mathbb{1}\{k_i \neq 0\}}, \end{aligned} \quad (10)$$

where t_i^r is the observed remaining follow-up time from the latest measurement, k_i is the observed event type of patient i , and β is a set of trainable weights in cause-specific decoder

modules and the subsequent fully connected neural network (i.e. $d_\beta(\cdot)$). Note that the likelihood contribution from a right-censored patient (i.e. those with $k_i = 0$) is that they are alive at t_i^r , which corresponds to the event free survival probability $S(t_i^r | Z_i)$ (see Equation 7).

Therefore, the total loss we want to minimize is

$$L_{\text{total}}(\mathcal{D}; \Phi, \zeta, \beta) = -\text{ELBO}(\mathcal{X}; \Phi, \zeta) - \log(L_{\text{surv}}(\mathcal{D}; \Phi, \beta)). \quad (11)$$

We perform an end-to-end training and utilize a standard back-propagation method to update weights in each module. For ODE solvers, we use the fifth order Dormand–Prince method (Dormand and Prince, 1980) from `tochdiffeq` Python package (Chen et al., 2018). Alternatively, the adjoint method, proposed in Chen et al. (2018), can be used to compute more memory-efficient gradients for ODE solvers, but at a cost of longer computation time.

4. Experiments

4.1. Setup

To demonstrate clinical utility of our model, we evaluated SurvLatent ODE on two real-world observational datasets: MIMIC-III for predicting time to hospital mortality (i.e. single-outcome) and the data from the Dana-Farber Cancer Institute (DFCI) for predicting time to DVT with all-cause mortality as a competing event. The datasets include routinely collected longitudinal measurements of patients’ biomarkers where some measurements are often informatively missing. For both prediction tasks, patients were aligned at the first measurement time upon their admission and time-to-event predictions were made from patients’ latest observations. Finally, we randomly split each data into a training set (55%), validation set (15%), and test set (30%), tuned hyperparameters using train and validation sets (see Section 4.5), and obtained model performances on the held-out test set across 25th, 50th, and 75th percentiles of corresponding event times.

4.2. Datasets

MIMIC-III MIMIC-III is a large, publicly available longitudinal dataset of patients who were admitted to critical care units (CCU) at the Beth Israel Deaconess Medical Center in Boston, Massachusetts (Johnson et al., 2016). In critical care scenarios, it is important to accurately identify high-risk patients as well as patient-specific time to mortality based on their time-varying biomarkers. This allows clinicians to determine the right level of care for patients in a timely manner based on their estimated risks and improve health outcomes while reducing unnecessary resource utilization.

For predicting time to hospital mortality, we utilized the cohort which consists of patients who were at risk after the first 36 hours of CCU admission ($n = 21,728$) and estimated their remaining time to mortality based on a total of 42 features. The features include static covariates such as age and sex as well as time-varying covariates such as vital signs and laboratory tests across the first 36 hours at a time resolution of 1 hour. For the longitudinal covariates, we included the top 40 most frequent vital signs and laboratory test results (see Appendix B for the full set of features). As an outcome, we used the time to hospital mortality measured from the 36th hour in the CCU while right-censoring those who did

not experience the mortality at their hospital discharge time. Among the total of 21,728 patients in our cohort, 2,281 patients (10.5 %) died at the hospital.

Dana-Farber Cancer Institute (DFCI) dataset Deep Vein Thrombosis (DVT) is a frequent, yet fatal complication in patients with active cancer, especially while they are receiving chemotherapy. DVT is associated with worse clinical outcomes such as elevated risk of mortality and reduced quality of life, and may lead to a significant disturbance of cancer treatment regimens (Blom et al., 2006; Khorana et al., 2007; Lloyd et al., 2018). For ambulatory cancer patients, preventive anti-thrombotic measures such as thromboprophylaxis, a mechanical method to promote venous outflow, and anticoagulants drugs are effective at reducing the incidence of DVT (Rutjes et al., 2020; Key et al., 2020; Xiong, 2021), however with an increased risk of bleeding (Key et al., 2020). Therefore, accurate stratification of the DVT risk among patients with cancer may allow clinicians to improve clinical outcome while minimizing side effects due to overtreatment.

The dataset includes patients with active cancer who were admitted to the DFCI from 2/12/2013 to 12/14/2021 and received targeted panel sequencing of their tumor biopsy. We set the sequence date for each patient as the prediction time to avoid immortal time bias. For the experiment cohort, we included those who received the sequencing within a year of their admission and were at the risk of DVT without any recorded prior DVT event (n = 8,734). The total number of features is 64, and the features include static covariates such as age, sex, presence of metastasis, and diagnosed cancer types as well as time-varying covariates such as laboratory test results and body mass index (BMI) across the first year from admission at a time resolution of one day (see Appendix B for the full set of features). We utilized ICD-10 diagnosis codes, I82.4 and I82.6, to determine the time of the venous thromboembolism (VTE) onset and I26 to determine the time of pulmonary embolism (PE) onset. And, we combined VTE and PE onset as the DVT event. We used the National Death Index (NDI) up until 12/31/2020 and the in-house death registry after the date to determine time of mortality. Finally, we right-censored patients at their last hospital visits, who did not experience DVT and death events. The demographics summary of the chosen cohort as well as causes of death (Table 4 and 5) are shown in Appendix C.

The main goal of this experiment was to develop an individualized risk score for cancer-related DVT by accurately estimating the time to DVT event in the presence of a competing risk for death as well as missing measurements and loss to follow-ups. We thus estimated a patient specific remaining time to DVT from the sequence date with all-cause mortality as a competing event. Finally, to demonstrate clinical utility of the proposed model, we benchmarked against the categorical Khorana score (Khorana et al., 2008), which is the current clinical standard for cancer-related DVT stratification and utilizes four clinical measurements together with cancer type (see Section 4.3 for details).

4.3. Baselines

Surv VAE-RNN adopts a variational autoencoder framework where both encoder and decoder are recurrent neural networks. For missing measurements, we utilized GRU-D (Che et al., 2018) approach where missing patterns as well as time intervals are concatenated to the input and dynamics of the hidden states are described by an exponential decay function.

This approach is closest to the proposed model except that in our model we utilized deep neural networks to learn the hidden state dynamics.

Recurrent Deep Survival Machine (RDSM, Nagpal et al. (2021a)) is a fully parametric time-to-event model where it learns representation of the input longitudinal data using a RNN-based model and derives the conditional survival distribution (i.e. $P(T^r = t|X)$) as a fixed mixture of parametric distributions (e.g. Weibull or Log-Normal). In this model, missing measurements are imputed using population means. The model cannot handle competing risks on its own.

Dynamic-Deephit (Lee et al., 2018b) is a discrete time-to-event model which, like RDSM, learns input representation using a RNN-based model and non-parametrically estimates the conditional joint distribution of the survival time and event type (i.e. $P(T = t, K = k|X)$). The model handles missing measurements by concatenating a vector of binary indicators for missing covariates as well as a vector of time intervals between two adjacent measurements into each input vector.

Cox Proportional Hazard model (Cox PH), proposed by Cox (1972), is a popular semi-parametric, time-to-event model which relates log of the relative hazard to a linear function of baseline features. For the experiment with the MIMIC dataset, we forward-filled the missing values at the 36th hour after CCU admission (i.e. prediction time) to obtain the baseline features. We used population means for the group of patients who do not have any measurement available

Khorana score (Khorana et al., 2008) is a simple linear scoring rule widely used in hospitals to predict future risk of DVT for patients with cancer. The score ranges from 0 to 6 and is computed based on the patient’s cancer type, body mass index (BMI), and lab test results including pre-chemotherapy platelet count, hemoglobin level, and pre-chemotherapy leukocyte count. 1,031 patients among the test cohort ($n = 2,630$) have the relevant features to compute Khorana scores at the prediction time. To obtain Khorana scores for the rest of patients in the test cohort, we imputed the features for those without BMI measurements and/or the relevant lab test results at the prediction time using population means.

Cause-specific Cox model (CS Cox) is a Cox PH based model for handling competing risks and captures effects of the static baseline features on the cause-specific hazard function for each event (Putter et al., 2007). Similar to the Cox PH setting above, we forward-filled the missing values at the prediction time.

Fine-Gray Cox model (FG Cox), proposed by Fine and Gray (1999), is another Cox PH based model, widely used for competing risks. The model directly captures effects of the baseline features on the cumulative incidence function to make survival predictions. We adopted the missing measurement imputation strategy exactly identical to CS Cox.

4.4. Evaluation Metrics

Time-dependent cumulative/dynamic AUC corresponds to the probability that, given a pair of patients where one experienced the event of interest before t and the other is event-free at t , the model correctly ranks their risks of the event (Kamarudin et al., 2017). The AUC for event k at time t is estimated as follows

$$\widehat{\text{AUC}}_k(t) = \frac{\sum_{(i,j) \in \mathcal{C}(t)} w_i \mathbb{1}(\hat{F}_k(t|X_j) \leq \hat{F}_k(t|X_i))}{\sum_{(i,j) \in \mathcal{C}(t)} w_i}, \quad (12)$$

where $\mathcal{C}(t)$ is a set of all comparable pairs at time t in the test cohort (i.e. $\mathcal{C}(t) = \{(i, j) \mid \mathbb{1}(t_i^r \leq t, t_j^r > t, k_i = k)\}$ where t_i^r corresponds to a remaining time to event for patient i who experiences event k before t , t_j^r correspond to a remaining time to event for patient j free of any events at t in a competing risks setting, and w_i are inverse probability of censoring weights for patient i , non-parametrically estimated by the Kaplan-Meier estimator. Under the independent censoring assumption, Equation (12) provides consistent estimation of the AUC (Uno et al., 2007; Blanche et al., 2013; Lambert and Chevret, 2016). We utilized `sksurv` Python package implementation of time-dependent AUC (Pösterl, 2020).

Time-dependent Brier Score is a generalization of the conventional Brier score (Brier, 1950) which can account for the right-censored data and measures the mean squared error at a given time point t . We extended the proposed formula in Graf et al. (1999) to measure the time-dependent Brier score for event k in a competing risks setting as follows

$$\text{BS}_k(t) = \frac{1}{N_t} \sum_{i=1}^{N_t} \mathbb{1}(t_i^r \leq t, k_i = k) (1 - \hat{F}_k(t|\mathcal{X}_i))^2 w_i + \mathbb{1}(t_i^r > t) (0 - \hat{F}_k(t|\mathcal{X}_i))^2 w_i, \quad (13)$$

where N_t is the number of patients in the held-out test set. This metric evaluates the model's calibration as well as discrimination performance (Xiu et al., 2020). We utilized `sksurv` Python package implementation of the time-dependent Brier score (Pösterl, 2020).

4.5. Hyperparameters

We used the validation set for optimizing hyperparameters and utilizing early-stopping to avoid over-fitting. We utilized a random search (Bergstra and Bengio, 2012), with the set of hyperparameters including dimensionality in the encoder and decoder networks, the number of nodes in RNN hidden layers, the number of hidden layers and nodes in fully-connected neural networks for ODEs. For a fair comparison, we similarly tuned the deep learning baseline models including Surv RNN-VAE, RDSM, and Dynamic-Deephit. See Appendix B for the full list of hyperparameters and their possible values across all models.

5. Results on Real Data

5.1. Results on MIMIC-III

As shown in Table 1, for the MIMIC dataset, SurvLatent ODE significantly outperformed the baseline models including recently published deep learning based approaches across all survival percentiles in the discriminative metric, while showing competitive performance in calibration captured by the Brier Score. The Cox PH model had the lowest discriminative performance, as it enforced a linear relationship between the set of covariates and did not incorporate the evolution of time-varying covariates. As an ablation study, we noticed that Surv RNN-VAE, which closely resembles the proposed model except how hidden dynamics are modeled (i.e. parameterized exponential decay vs. neural networks), showed fairly poor performance across all metrics. This demonstrates that a Neural-ODE based approach allows the variational autoencoder framework to be successfully implemented for time-to-event modeling of longitudinal data, which would have been infeasible otherwise.

| | Time-dependent AUC(t) | | | Brier Score, BS(t) | | |
|--|------------------------------|------------------------------|-------------------------------|------------------------------|------------------------------|-------------------------------|
| | 25th percentile (Hour 35) | 50th percentile (Hour 81) | 75th percentile (Hour 150) | 25th percentile (Hour 35) | 50th percentile (Hour 81) | 75th percentile (Hour 150) |
| SurvLatent ODE (Proposed model) | 0.920 (0.009) | 0.883 (0.009) | 0.831 (0.010) | 0.0220 (0.0013) | 0.0442 (0.0019) | 0.0789 (0.0029) |
| Surv RNN-VAE | 0.535 (0.022)** | 0.535 (0.016)** | 0.521 (0.014)** | 0.0281 (0.0017)** | 0.0571 (0.0023)** | 0.0950 (0.003)** |
| RDSM | 0.836 (0.017)** | 0.817 (0.013)** | 0.784 (0.011)** | 0.0241 (0.0018)* | 0.0449 (0.0023) | 0.0618 (0.0025) |
| Dynamic-Deephit | 0.891 (0.009)** | 0.860 (0.009)* | 0.808 (0.010)* | 0.0247 (0.0018)* | 0.0492 (0.0024)** | 0.0816 (0.0032) |
| Cox PH | 0.826 (0.017)** | 0.806 (0.013)** | 0.762 (0.012)** | 0.0234 (0.0017) | 0.0465 (0.0023) | 0.0789 (0.0032) |

Table 1: Performance summary of the models across the 25th, 50th, and 75th percentiles of event times on the held-out test set of MIMIC-III data ($n = 6,519$) for predicting **time to hospital mortality**. Time-dependent AUC (higher the better) as well as Brier scores (lower the better) are used as evaluation metrics (see Section 4.4). Standard errors, obtained from the non-parametric bootstrap on the test cohort, are shown in parenthesis. We obtained statistical significance (* : $p < 0.05$, ** : $p < 0.001$) by estimating mean of differences in performance between the proposed model (SurvLatent ODE) and each baseline model across bootstrap iterations and performing a one-sided test.

5.2. Results on DVT

As shown in Table 2 and 3, SurvLatent ODE significantly outperformed all the baseline models including Dynamic-Deephit in the discriminative as well as the calibration metrics, with a statistically significant improvement over the next-best method in two out of three time horizons for the discriminative performance. For predicting time to all-cause mortality (i.e. the competing event), SurvLatent ODE again outperformed all the baseline models in the discriminative metric, with statistically significant improvement for two out of three time horizons, while achieving competitive but weaker performance in the calibration metric. Specifically, Dynamic-Deephit showed superior calibration at the short survival quantile (25%) while the Fine-Gray Cox model (FG Cox) showed superior calibration for the longer survival quantiles (50% and 75%).

| | Time-dependent AUC $_k(t)$ | | | Brier Score, BS $_k(t)$ | | |
|--|-----------------------------|------------------------------|------------------------------|-----------------------------|------------------------------|------------------------------|
| | 25th percentile (Day 47) | 50th percentile (Day 113) | 75th percentile (Day 266) | 25th percentile (Day 47) | 50th percentile (Day 113) | 75th percentile (Day 266) |
| SurvLatent ODE (Proposed model) | 0.782 (0.031) | 0.781 (0.021) | 0.758 (0.020) | 0.0222 (0.0026) | 0.0426 (0.0034) | 0.0631 (0.0040) |
| Dynamic-Deephit | 0.729 (0.032)* | 0.770 (0.023) | 0.722 (0.022)* | 0.0223 (0.0027) | 0.0428 (0.0036) | 0.0641 (0.0042)* |
| CS Cox | 0.702 (0.034)* | 0.728 (0.023)* | 0.706 (0.020)* | 0.0228 (0.0028) | 0.0444 (0.0038)* | 0.0666 (0.0045)** |
| FG Cox | 0.672 (0.033)* | 0.695 (0.024)* | 0.686 (0.019)** | 0.0227 (0.0028) | 0.0445 (0.0038)* | 0.0667 (0.0045)** |
| Khorana scores ¹ | 0.625 (0.051) | 0.592 (0.036) | 0.581 (0.029) | N/A | N/A | N/A |
| Khorana scores (imputed) | 0.627 (0.036)** | 0.628 (0.026)** | 0.628 (0.022)** | N/A | N/A | N/A |

Table 2: Performance summary of the models across the 25th, 50th, and 75th percentiles of event times on the held-out test set of the in-house DFCI data ($n = 2,630$) for predicting **time to DVT event** with an all-cause mortality as a competing event. Time-dependent AUC (higher the better) as well as Brier scores (lower the better) are used as evaluation metrics. Standard errors, shown in parenthesis, as well as statistical significance (* : $p < 0.05$, ** : $p < 0.001$) were obtained exactly in the same manner as in the MIMIC-III experiment (see Table 1 caption). Note that Khorana score adopts the integer scoring system and its survival calibration performance cannot be evaluated.

1. As mentioned in Section 4.3, this cohort includes 1,031 patients with recorded relevant lab test results and BMI to compute Khorana scores at the prediction time (i.e. panel sequencing data).

| | Time-dependent AUC _k (t) | | | Brier Score, BS _k (t) | | |
|-----------------|--|------------------------------|------------------------------|----------------------------------|------------------------------|------------------------------|
| | 25th percentile (Day 141) | 50th percentile (Day 269) | 75th percentile (Day 446) | 25th percentile (Day 141) | 50th percentile (Day 269) | 75th percentile (Day 446) |
| | SurvLatent ODE (Proposed model) | 0.772 (0.018) | 0.762 (0.014) | 0.761 (0.012) | 0.0785 (0.0028) | 0.1270 (0.0031) |
| Dynamic-Deephit | 0.762 (0.018) | 0.742 (0.014)* | 0.741 (0.012)** | 0.0662 (0.0041) | 0.1198 (0.0047) | 0.1600 (0.0044) |
| CS Cox | 0.711 (0.020)** | 0.710 (0.014)** | 0.710 (0.013)** | 0.0675 (0.0046) | 0.1204 (0.0055) | 0.1602 (0.0054) |
| FG Cox | 0.706 (0.020)** | 0.706 (0.014)** | 0.706 (0.013)** | 0.0667 (0.0045) | 0.1179 (0.0050) | 0.1580 (0.0048) |

Table 3: Performance summary of the models across the 25th, 50th, and 75th percentiles of event times for predicting **time to all-cause mortality** as the competing event. Performances of each model for DVT (Table 2) and all-cause mortality (Table 3) were obtained from a single model evaluated on the same held-out test set of the in-house data ($n = 2,630$). Time-dependent AUC (higher the better) as well as Brier scores (lower the better) are used as evaluation metrics.

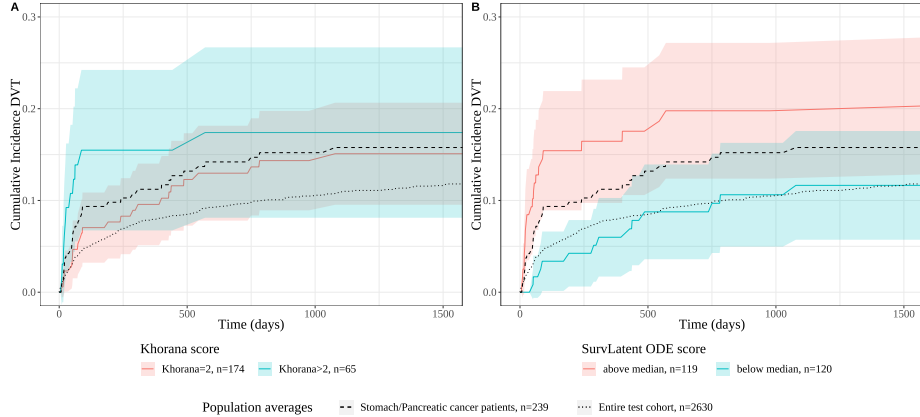


Figure 2: **Left** : Khorana-based stratification for patients diagnosed with pancreatic and stomach cancers ($n = 239$) among the held-out test set. By definition, these patients have at least a Khorana score of 2 due to their high-risk cancer types (Khorana et al., 2008). Cumulative incidence trajectories were estimated by Aalen–Johansen estimator (Johansen, 1978), a non-parametric estimator for cumulative incidence, taking into account competing risks. **Right** : the same cohort of patients was divided into two groups (i.e. above median and below median) based on their cause-specific restricted mean failure time (RMFT) (i.e. $\int_0^{365} \hat{F}_k(t|\mathcal{X}_i)dt$) estimated by SurvLatent ODE. SurvLatent ODE based score was able to capture heterogeneity within the elevated risk group for DVT.

SurvLatent ODE significantly outperformed the current clinical standard, Khorana scores (Khorana et al., 2008) for predicting time to DVT events across all percentiles (Table 2). Khorana scores range from 0 to 6 and are meant to stratify risk for DVT among patients with cancer based on 5 different features including diagnosed cancer type and lab test results (see Section 4.3 for details). The performance of Khorana scores was comparatively poor, even after the imputation. Importantly, SurvLatent ODE continued to outperform the Khorana score when focusing on the highest risk cancer types, pancreatic and stomach cancer, where DVT events are particularly high (Fig. 2). Indeed, SurvLatent ODE identified a low risk subpopulation that had event rates comparable to the population baseline (shown as a dotted line in Fig. 2), and substantially lower than the corresponding lowest Khorana score. In this set-up, to stratify risk groups at the prediction time, we computed the cause-specific restricted mean failure time (RMFT) from Day 0 (prediction date) to Day 365

(i.e. $\int_0^{365} \hat{F}_k(t|\mathcal{X}_i)dt$), which is interpreted as the expected number of days lost due to cause k before Day 365 (Mozumder et al., 2021). Furthermore, the proposed model demonstrated a strong performance across various subsets of patients defined by diagnosed cancer types and cancer stage (see Appendix C).

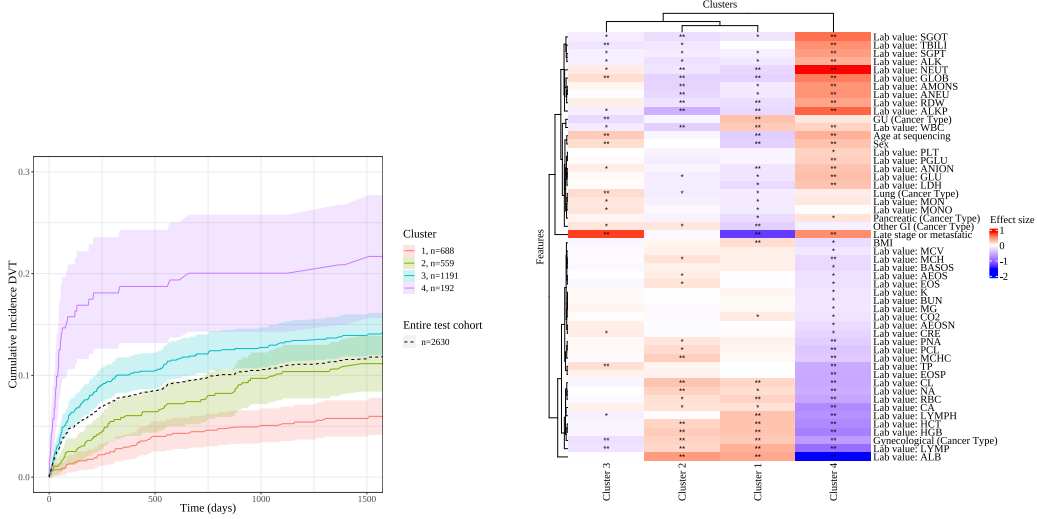


Figure 3: **Left** : Cumulative Incidence trajectories for the DVT event across the latent clusters. The cumulative incidence trajectories were estimated by the Aalen-Johansen Estimator (Johansen, 1978). **Right** : Heatmap visualization of feature-wise coefficient for each latent cluster. See Appendix C for detailed description of the method. SurvLatent ODE provided clinically meaningful and interpretable latent states. Features significantly associated with Cluster 4 include well-established risk factors for DVT. Note that * : $p < 0.05$, ** : $p < 0.001$ for statistical significance of feature coefficient.

As shown in Fig. 3, SurvLatent ODE provided clinically meaningful and interpretable latent states with the obtained latent clusters ($k = 4$) exhibiting significantly different DVT risk trajectories. The latent state for each patient was obtained from the output of the cause-specific decoder for the DVT event (see Appendix C for more detail). We obtained a cluster specific coefficient for each baseline feature by running a logistic regression with cluster membership as the binary outcome. Khorana scores were also included as a categorical covariate to highlight the contribution of features beyond the current clinical guidelines. Well-established DVT risk factors were associated with the highest risk cluster (i.e. Cluster 4), including cancer type (e.g. pancreatic cancer) and known lab test results (platelet count : PLT, hemoglobin level : HGB, and white blood cell count : WBC) with consistent directions (Khorana et al., 2008). While some of these factors are included in the Khorana score, the fact that they were still significantly associated after conditioning on the Khorana score indicates that SurvLatent ODE identified additional latent trajectory variations among these factors. In addition to the features for the Khorana score, we observed associations with neutrophils (NEUT), albumins (ALB), and SGOT which were supported by the literature (Kapoor et al., 2018; Folsom et al., 2010, 2014).

6. Discussion

We propose a full ODE-based variational autoencoder time-to-event framework for modeling longitudinal data, which enables an effective parameterization of the dynamics in the representation space of the input temporal data under missing values. Combined with the flexible non-parametric estimation of cause-specific hazard functions for multiple events, our proposed model outperforms the baselines including recently published deep-learning based models in two real-world datasets. Our proposed method offers a promising deep-learning based time-to-event framework for risk predictions in healthcare scenarios where data irregularities such as missing measurements and loss to follow-up are very common.

Our model significantly outperforms the current clinical standard, Khorana scores, for predicting the DVT event among patients with cancer. In addition, by learning complex non-linear relationships between time-varying features, our model makes accurate survival predictions for a wider range of patients while effectively capturing heterogeneity of the DVT risk, including identifying low-risk patients in conventionally high-risk cancer types. As future clinically-oriented work, we consider incorporating major fixed-effect variables, such as patient’s tumor genetics, as well as more granular outcomes such as stroke, myocardial infarction, and cancer disease progression.

On the technical side, future work may involve estimating well-calibrated uncertainty of survival curves, reflective of training data availability for a given task as well as sample-wise prediction difficulty. One can potentially achieve this by incorporating the survival likelihood into the ELBO formulation. In addition, as demonstrated in [Garnelo et al. \(2018\)](#); [Norcliffe et al. \(2021\)](#), one can explicitly capture uncertainty over underlying dynamics and render survival estimates aware of the uncertainty in the dynamics. From the survival modeling perspective, it is of interest to additionally adopt the sub-distribution hazard framework which models effects of covariates on cause-specific cumulative incidence functions and is often used for an individual risk prediction ([Austin et al., 2016](#); [Berger et al., 2020](#)).

Acknowledgments

This work was supported by NIH R01 CA227237, Louis B. Mayer Foundation, DDCF Clinical Scientist Development Award, Phi Beta Psi Sorority, and The Emerson Collective.

References

Ahmed M. Alaa and Mihaela van der Schaar. Deep multi-task gaussian processes for survival analysis with competing risks. In I. Guyon, U. V. Luxburg, S. Bengio, H. Wallach, R. Fergus, S. Vishwanathan, and R. Garnett, editors, *Advances in Neural Information Processing Systems*, volume 30. Curran Associates, Inc., 2017. URL <https://proceedings.neurips.cc/paper/2017/file/861dc9bd7f4e7dd3cccd534d0ae2a2e9-Paper.pdf>.

Peter C. Austin, Douglas S. Lee, and Jason P. Fine. Introduction to the analysis of survival data in the presence of competing risks. *Circulation*, 133(6):601–609, 2016. doi: 10.1161/circulationaha.115.017719.

M. Berger, M. Schmid, T. Welchowski, S. Schmitz-Valckenberg, and J. Beyersmann. Subdistribution hazard models for competing risks in discrete time. *Biostatistics*, 21(3):449–466, 07 2020.

James Bergstra and Yoshua Bengio. Random search for hyper-parameter optimization. *J. Mach. Learn. Res.*, 13:281–305, 2012. URL <http://dblp.uni-trier.de/db/journals/jmlr/jmlr13.html#BergstraB12>.

S. D. Berry, L. Ngo, E. J. Samelson, and D. P. Kiel. Competing risk of death: an important consideration in studies of older adults. *J Am Geriatr Soc*, 58(4):783–787, Apr 2010.

Christopher M. Bishop. *Pattern Recognition and Machine Learning (Information Science and Statistics)*. Springer-Verlag, Berlin, Heidelberg, 2006. ISBN 0387310738.

Paul Blanche, Jean-François Dartigues, and Hélène Jacqmin-Gadda. Estimating and comparing time-dependent areas under receiver operating characteristic curves for censored event times with competing risks. *Statistics in Medicine*, 32(30):5381–5397, Dec 2013. ISSN 02776715. doi: 10.1002/sim.5958. URL <https://onlinelibrary.wiley.com/doi/10.1002/sim.5958>.

J. W. Blom, J. P. Vanderschoot, M. J. Oostindier, S. Osanto, F. J. van der Meer, and F. R. Rosendaal. Incidence of venous thrombosis in a large cohort of 66,329 cancer patients: results of a record linkage study. *J Thromb Haemost*, 4(3):529–535, Mar 2006.

Glenn W. Brier. Verification of forecasts expressed in terms of probability. *Monthly Weather Review*, 78(1):1–3, Jan 1950. ISSN 0027-0644, 1520-0493. doi: 10.1175/1520-0493(1950)078<0001:VOFEIT>2.0.CO;2. URL [http://journals.ametsoc.org/doi/10.1175/1520-0493\(1950\)078<0001:VOFEIT>2.0.CO;2](http://journals.ametsoc.org/doi/10.1175/1520-0493(1950)078<0001:VOFEIT>2.0.CO;2).

Rich Caruana. Multitask learning. *Mach. Learn.*, 28(1):41–75, jul 1997. ISSN 0885-6125. doi: 10.1023/A:1007379606734. URL <https://doi.org/10.1023/A:1007379606734>.

Zhengping Che, Sanjay Purushotham, Kyunghyun Cho, David Sontag, and Yan Liu. Recurrent Neural Networks for Multivariate Time Series with Missing Values. *Scientific Reports*, 8(1):6085, December 2018. ISSN 2045-2322. doi: 10.1038/s41598-018-24271-9. URL <http://www.nature.com/articles/s41598-018-24271-9>.

Ricky T. Q. Chen, Yulia Rubanova, Jesse Bettencourt, and David K Duvenaud. Neural ordinary differential equations. In S. Bengio, H. Wallach, H. Larochelle, K. Grauman, N. Cesa-Bianchi, and R. Garnett, editors, *Advances in Neural Information Processing Systems*, volume 31. Curran Associates, Inc., 2018. URL <https://proceedings.neurips.cc/paper/2018/file/69386f6bb1dfed68692a24c8686939b9-Paper.pdf>.

Kyunghyun Cho, Bart van Merriënboer, Dzmitry Bahdanau, and Yoshua Bengio. On the properties of neural machine translation: Encoder-decoder approaches, 2014.

Edward Choi, Mohammad Taha Bahadori, Andy Schuetz, Walter F. Stewart, and Jimeng Sun. Doctor ai: Predicting clinical events via recurrent neural networks, 2016.

D. R. Cox. Regression models and life-tables. *Journal of the Royal Statistical Society: Series B (Methodological)*, 34(2):187–202, January 1972. doi: 10.1111/j.2517-6161.1972.tb00899.x. URL <https://doi.org/10.1111/j.2517-6161.1972.tb00899.x>.

J.R. Dormand and P.J. Prince. A family of embedded runge-kutta formulae. *Journal of Computational and Applied Mathematics*, 6(1):19–26, Mar 1980. ISSN 03770427. doi: 10.1016/0771-050X(80)90013-3. URL <https://linkinghub.elsevier.com/retrieve/pii/0771050X80900133>.

Jason P. Fine and Robert J. Gray. A Proportional Hazards Model for the Subdistribution of a Competing Risk. *Journal of the American Statistical Association*, 94(446):496–509, June 1999. ISSN 0162-1459, 1537-274X. doi: 10.1080/01621459.1999.10474144. URL <http://www.tandfonline.com/doi/abs/10.1080/01621459.1999.10474144>.

A. R. Folsom, P. L. Lutsey, S. R. Heckbert, and M. Cushman. Serum albumin and risk of venous thromboembolism. *Thromb Haemost*, 104(1):100–104, Jul 2010.

A. R. Folsom, P. L. Lutsey, N. S. Roetker, W. D. Rosamond, M. Lazo, S. R. Heckbert, S. Basu, M. Cushman, and E. Selvin. Elevated hepatic enzymes and incidence of venous thromboembolism: a prospective study. *Ann Epidemiol*, 24(11):817–821, Nov 2014.

Joseph Futoma, Sanjay Hariharan, Mark Sendak, Nathan Brajer, Meredith Clement, Armando Bedoya, Cara O’Brien, and Katherine Heller. An improved multi-output gaussian process rnn with real-time validation for early sepsis detection, 2017.

Marta Garnelo, Dan Rosenbaum, Christopher Maddison, Tiago Ramalho, David Saxton, Murray Shanahan, Yee Whye Teh, Danilo Rezende, and S. M. Ali Eslami. Conditional neural processes. In Jennifer Dy and Andreas Krause, editors, *Proceedings of the 35th International Conference on Machine Learning*, volume 80 of *Proceedings of Machine Learning Research*, pages 1704–1713. PMLR, 10–15 Jul 2018. URL <https://proceedings.mlr.press/v80/garnelo18a.html>.

Erika Graf, Claudia Schmoor, Willi Sauerbrei, and Martin Schumacher. Assessment and comparison of prognostic classification schemes for survival data. *Statistics in Medicine*, 18(17–18):2529–2545, Sep 1999. ISSN 0277-6715, 1097-0258. doi: 10.1002/(SICI)1097-0258(19990915/30)18:17/18<2529::AID-SIM274>3.0.CO;2-5. URL [https://onlinelibrary.wiley.com/doi/10.1002/\(SICI\)1097-0258\(19990915/30\)18:17/18<2529::AID-SIM274>3.0.CO;2-5](https://onlinelibrary.wiley.com/doi/10.1002/(SICI)1097-0258(19990915/30)18:17/18<2529::AID-SIM274>3.0.CO;2-5).

Stefan Groha, Sebastian M. Schmon, and Alexander Gusev. A General Framework for Survival Analysis and Multi-State Modelling. *arXiv:2006.04893 [cs, stat]*, February 2021. URL <http://arxiv.org/abs/2006.04893>. arXiv: 2006.04893.

Daniel Jarrett, Jinsung Yoon, and Mihaela van der Schaar. Match-net: Dynamic prediction in survival analysis using convolutional neural networks. *CoRR*, abs/1811.10746, 2018. URL <http://arxiv.org/abs/1811.10746>.

Ren Johansen. An empirical transition matrix for non-homogeneous markov chains based on censored observations. 1978.

A. E. Johnson, T. J. Pollard, L. Shen, L. W. Lehman, M. Feng, M. Ghassemi, B. Moody, P. Szolovits, L. A. Celi, and R. G. Mark. MIMIC-III, a freely accessible critical care database. *Sci Data*, 3:160035, May 2016.

Adina Najwa Kamarudin, Trevor Cox, and Ruwanthi Kolamunnage-Dona. Time-dependent roc curve analysis in medical research: current methods and applications. *BMC Medical Research Methodology*, 17(1):53, Dec 2017. ISSN 1471-2288. doi: 10.1186/s12874-017-0332-6. URL <http://bmcmedresmethodol.biomedcentral.com/articles/10.1186/s12874-017-0332-6>.

S. Kapoor, A. Opneja, and L. Nayak. The role of neutrophils in thrombosis. *Thromb Res*, 170:87–96, 10 2018.

J. L. Katzman, U. Shaham, A. Cloninger, J. Bates, T. Jiang, and Y. Kluger. DeepSurv: personalized treatment recommender system using a Cox proportional hazards deep neural network. *BMC Med Res Methodol*, 18(1):24, 02 2018.

N. S. Key, A. A. Khorana, N. M. Kuderer, K. Bohlke, A. Y. Y. Lee, J. I. Arcelus, S. L. Wong, E. P. Balaban, C. R. Flowers, C. W. Francis, L. E. Gates, A. K. Kakkar, M. N. Levine, H. A. Liebman, M. A. Tempero, G. H. Lyman, and A. Falanga. Venous Thromboembolism Prophylaxis and Treatment in Patients With Cancer: ASCO Clinical Practice Guideline Update. *J Clin Oncol*, 38(5):496–520, 02 2020.

A. A. Khorana, C. W. Francis, E. Culakova, N. M. Kuderer, and G. H. Lyman. Thromboembolism is a leading cause of death in cancer patients receiving outpatient chemotherapy. *J Thromb Haemost*, 5(3):632–634, Mar 2007.

A. A. Khorana, N. M. Kuderer, E. Culakova, G. H. Lyman, and C. W. Francis. Development and validation of a predictive model for chemotherapy-associated thrombosis. *Blood*, 111(10):4902–4907, May 2008.

Diederik P Kingma and Max Welling. Auto-encoding variational bayes, 2013. URL <https://arxiv.org/abs/1312.6114>.

Jérôme Lambert and Sylvie Chevret. Summary measure of discrimination in survival models based on cumulative/dynamic time-dependent roc curves. *Statistical Methods in Medical Research*, 25(5):2088–2102, Oct 2016. ISSN 0962-2802, 1477-0334. doi: 10.1177/0962280213515571. URL <http://journals.sagepub.com/doi/10.1177/0962280213515571>.

C. Lee, J. Yoon, and M. V. Schaar. Dynamic-DeepHit: A Deep Learning Approach for Dynamic Survival Analysis With Competing Risks Based on Longitudinal Data. *IEEE Trans Biomed Eng*, 67(1):122–133, 01 2020.

Changhee Lee, William Zame, Jinsung Yoon, and Mihaela van der Schaar. DeepHit: A Deep Learning Approach to Survival Analysis With Competing Risks. *Proceedings of the AAAI Conference on Artificial Intelligence*, 32(1), April 2018a. URL <https://ojs.aaai.org/index.php/AAAI/article/view/11842>.

M. Lee, E. J. Feuer, and J. P. Fine. On the analysis of discrete time competing risks data. *Biometrics*, 74(4):1468–1481, 12 2018b.

Zachary C Lipton, David C Kale, and Randall Wetzel. Modeling Missing Data in Clinical Time Series with RNNs. page 17, 2016.

A. J. Lloyd, S. Dewilde, S. Noble, E. Reimer, and A. Y. Y. Lee. What Impact Does Venous Thromboembolism and Bleeding Have on Cancer Patients’ Quality of Life? *Value Health*, 21(4):449–455, 04 2018.

Md. Maniruzzaman, Md. Jahanur Rahman, Md. Al-MehediHasan, Harman S. Suri, Md. Menhazul Abedin, Ayman El-Baz, and Jasjit S. Suri. Accurate diabetes risk stratification using machine learning: Role of missing value and outliers. *Journal of Medical Systems*, 42(5):92, May 2018. ISSN 0148-5598, 1573-689X. doi: 10.1007/s10916-018-0940-7. URL <http://link.springer.com/10.1007/s10916-018-0940-7>.

Xenia Misicouridou, Adler Perotte, Noemie Elhadad, and Rajesh Ranganath. Deep survival analysis: Nonparametrics and missingness. In Finale Doshi-Velez, Jim Fackler, Ken Jung, David Kale, Rajesh Ranganath, Byron Wallace, and Jenna Wiens, editors, *Proceedings of the 3rd Machine Learning for Healthcare Conference*, volume 85 of *Proceedings of Machine Learning Research*, pages 244–256. PMLR, 17–18 Aug 2018. URL <https://proceedings.mlr.press/v85/misicouridou18a.html>.

S. I. Mozumder, M. J. Rutherford, and P. C. Lambert. Estimating restricted mean survival time and expected life-years lost in the presence of competing risks within flexible parametric survival models. *BMC Med Res Methodol*, 21(1):52, 03 2021.

Paul D. Myers, Benjamin M. Scirica, and Collin M. Stultz. Machine learning improves risk stratification after acute coronary syndrome. *Scientific Reports*, 7(1):12692, Dec 2017. ISSN 2045-2322. doi: 10.1038/s41598-017-12951-x. URL <http://www.nature.com/articles/s41598-017-12951-x>.

Chirag Nagpal, Vincent Jeanselme, and Artur Dubrawski. Deep parametric time-to-event regression with time-varying covariates. In Russell Greiner, Neeraj Kumar, Thomas Alexander Gerds, and Mihaela van der Schaar, editors, *Proceedings of AAAI Spring Symposium on Survival Prediction - Algorithms, Challenges, and Applications 2021*, volume 146 of *Proceedings of Machine Learning Research*, pages 184–193. PMLR, 22–24 Mar 2021a. URL <http://proceedings.mlr.press/v146/nagpal21a.html>.

Chirag Nagpal, Steve Yadlowsky, Negar Rostamzadeh, and Katherine Heller. Deep cox mixtures for survival regression, 2021b.

Alexander Norcliffe, Cristian Bodnar, Ben Day, Jacob Moss, and Pietro Liò. Neural ode processes, 2021. URL <https://arxiv.org/abs/2103.12413>.

F. Pedregosa, G. Varoquaux, A. Gramfort, V. Michel, B. Thirion, O. Grisel, M. Blondel, P. Prettenhofer, R. Weiss, V. Dubourg, J. Vanderplas, A. Passos, D. Cournapeau, M. Brucher, M. Perrot, and E. Duchesnay. Scikit-learn: Machine learning in Python. *Journal of Machine Learning Research*, 12:2825–2830, 2011.

Sebastian Pölsterl. scikit-survival: A library for time-to-event analysis built on top of scikit-learn. *Journal of Machine Learning Research*, 21(212):1–6, 2020. URL <http://jmlr.org/papers/v21/20-729.html>.

H. Putter, M. Fiocco, and R. B. Geskus. Tutorial in biostatistics: competing risks and multi-state models. *Statistics in Medicine*, 26(11):2389–2430, May 2007. ISSN 02776715, 10970258. doi: 10.1002/sim.2712. URL <https://onlinelibrary.wiley.com/doi/10.1002/sim.2712>.

Rajesh Ranganath, Adler Perotte, Noémie Elhadad, and David Blei. Deep Survival Analysis. *arXiv:1608.02158 [cs, stat]*, September 2016. URL <http://arxiv.org/abs/1608.02158>. arXiv: 1608.02158.

Kan Ren, Jiarui Qin, Lei Zheng, Zhengyu Yang, Weinan Zhang, Lin Qiu, and Yong Yu. Deep recurrent survival analysis, 2018.

Yulia Rubanova, Ricky T. Q. Chen, and David K Duvenaud. Latent ordinary differential equations for irregularly-sampled time series. In H. Wallach, H. Larochelle, A. Beygelzimer, F. d'Alché-Buc, E. Fox, and R. Garnett, editors, *Advances in Neural Information Processing Systems*, volume 32. Curran Associates, Inc., 2019. URL <https://proceedings.neurips.cc/paper/2019/file/42a6845a557bef704ad8ac9cb4461d43-Paper.pdf>.

A. W. Rutjes, E. Porreca, M. Candeloro, E. Valeriani, and M. Di Nisio. Primary prophylaxis for venous thromboembolism in ambulatory cancer patients receiving chemotherapy. *Cochrane Database Syst Rev*, 12:CD008500, 12 2020.

Skipper Seabold and Josef Perktold. statsmodels: Econometric and statistical modeling with python. In *9th Python in Science Conference*, 2010.

Hossein Soleimani, James Hensman, and Suchi Saria. Scalable Joint Models for Reliable Uncertainty-Aware Event Prediction. *arXiv:1708.04757 [cs, stat]*, August 2017. URL <http://arxiv.org/abs/1708.04757>. arXiv: 1708.04757.

Weijing Tang, Jiaqi Ma, Qiaozhu Mei, and Ji Zhu. Soden: A scalable continuous-time survival model through ordinary differential equation networks, 2020.

Gerhard Tutz and Matthias Schmid. *Modeling Discrete Time-to-Event Data*. Springer Publishing Company, Incorporated, 1st edition, 2016. ISBN 3319281569.

Hajime Uno, Tianxi Cai, Lu Tian, and L. J Wei. Evaluating prediction rules for t -year survivors with censored regression models. *Journal of the American Statistical Association*, 102(478):527–537, Jun 2007. ISSN 0162-1459, 1537-274X. doi: 10.1198/016214507000000149. URL <http://www.tandfonline.com/doi/abs/10.1198/016214507000000149>.

W. Xiong. Current status of treatment of cancer-associated venous thromboembolism. *Thromb J*, 19(1):21, Mar 2021.

Zidi Xiu, Chenyang Tao, and Ricardo Henao. Variational learning of individual survival distributions. In *Proceedings of the ACM Conference on Health, Inference, and Learning*,

page 10–18. ACM, Apr 2020. ISBN 9781450370462. doi: 10.1145/3368555.3384454. URL <https://dl.acm.org/doi/10.1145/3368555.3384454>.

Daniel Zeiberg, Tejas Prahlad, Brahmajee K. Nallamothu, Theodore J. Iwashyna, Jenna Wiens, and Michael W. Sjoding. Machine learning for patient risk stratification for acute respiratory distress syndrome. *PLOS ONE*, 14(3):e0214465, Mar 2019. ISSN 1932-6203. doi: 10.1371/journal.pone.0214465. URL <https://dx.plos.org/10.1371/journal.pone.0214465>.

Appendix A. Discrete survival analysis

In Section 3.3.2, given that $T_i^r \perp\!\!\!\perp \mathcal{X}_i | Z_i$, we claim the following

$$S(t | \mathcal{X}_i, Z_i^t) = S(t | Z_i^t) = P(T_i^r > t | Z_i^t) = \prod_{\tau_{i,l} < \tau \leq t} \left(1 - \sum_{k=1}^K \lambda_{i,k}^*(\tau) \right).$$

Proof For a discrete event time T^r , we notice that

$$S(t | Z_i^t) = \prod_{\tau_{i,l} < \tau \leq t} \frac{S(\tau | Z_i^t)}{S(\tau - 1 | Z_i^t)}, \quad (14)$$

where $S(\tau | Z_i^t) = 1$ for $\tau \leq \tau_{i,l}$. And, we have

$$\begin{aligned} \lambda_{i,k}^*(t) &= P(T_i^r = t, k_i = k | T_i^r \geq t, \mathcal{X}_i, Z_i^t) \\ &= P(T_i^r = t, k_i = k | T_i^r \geq t, Z_i^t) \\ &= \frac{P(T_i^r = t, k_i = k | Z_i^t)}{P(T_i^r > t - 1 | Z_i^t)} \\ &= \frac{P(T_i^r = t, k_i = k | Z_i^t)}{S(t - 1 | Z_i^t)} \\ &= \frac{F_k(t | Z_i^t) - F_k(t - 1 | Z_i^t)}{S(t - 1 | Z_i^t)}. \end{aligned} \quad (15)$$

Summing up the hazard function across K events, we have

$$\sum_{k=1}^K \lambda_{i,k}^*(t) = \sum_{k=1}^K \frac{F_k(t | Z_i^t) - F_k(t - 1 | Z_i^t)}{S(t - 1 | Z_i^t)} = \frac{S(t - 1 | Z_i^t) - S(t | Z_i^t)}{S(t - 1 | Z_i^t)} = 1 - \frac{S(t | Z_i^t)}{S(t - 1 | Z_i^t)}. \quad (16)$$

Finally, rearranging Equation 16 and plugging it into Equation 14, we have

$$S(t | Z_i^t) = \prod_{\tau_{i,l} < \tau \leq t} \frac{S(\tau | Z_i^t)}{S(\tau - 1 | Z_i^t)} = \prod_{\tau_{i,l} < \tau \leq t} \left(1 - \sum_{k=1}^K \lambda_{i,k}^*(\tau) \right). \quad (17)$$

■

Appendix B. Model implementation

B.1. Full set of features

For MIMIC-III, we utilized a total of 42 features including 2 static covariates (age and gender) as well as top 40 most frequent time-varying vital signs and laboratory test results (heart rate, respiratory rate, systolic blood pressure, diastolic blood pressure, mean blood pressure, oxygen saturation, temperature, glucose, central venous pressure, hematocrit,

potassium, sodium, pulmonary artery pressure systolic, ph, hemoglobin, chloride, co2 (etco2, pco2, etc.), partial pressure of carbon dioxide, creatinine, blood urea nitrogen, bicarbonate, platelets, anion gap, white blood cell count, magnesium, positive end-expiratory pressure set, calcium, tidal volume observed, partial thromboplastin time, red blood cell count, mean corpuscular volume, prothrombin time inr, prothrombin time pt, fraction inspired oxygen set, peak inspiratory pressure, calcium ionized, phosphate, respiratory rate set, phosphorous, tidal volume set).

For the in-house data, we utilized a total of 62 features including 11 static covariates : age, sex, late stage/metastasis indicator, lung-related cancer, breast cancer, pancreatic cancer, thyroid cancer, other Gastrointestinal (GI) cancer, Cancer of Unknown Primary (CUP), Genitourinary (GU), and Gynecologic (gyn) and 51 time-varying covariates. The set of time-varying covariates include Body Mass Index (BMI) and various lab tests : PLCO2, PCL, BASO, HCT, MVP, CL, ANEU, EOSP, TP, PGLU, LDH, PLT, MONO, EOS, ALK, ALB, RDW, NEUT, ABASO, SGPT, CRE, ANION, LYMPH, MON, GFR, MCH, LYMP, MCHC, BUN, ALKP, HGB, BASOS, GLOB, K, PNA, AEOSN, MG, TBILI, CA, PK, AEOS, GLU, RBC, NA, CO2, AMONS, PBUN, WBC, MCV, SGOT.

B.2. Hyperparameter Tuning

We used the validation set for optimizing hyperparameters and utilizing early-stopping to avoid potential over-fitting. A random search (Bergstra and Bengio, 2012) was utilized for each deep learning based model on the following set of hyperparameters :

SurvLatent ODE (Proposed model) Latent trajectory (Z^t) dimension : [32, 36, 40], Input embedding dimension : [40, 50, 60, 70], Number of layers in the encoder ODE function, $f_\gamma(\cdot)$: [3, 5, 7], Number of layers in the decoder ODE function, $g_\phi(\cdot)$: [3, 5, 7], Hidden units in $f_\gamma(\cdot)$ and $g_\phi(\cdot)$: [30, 50, 70], Hidden units in GRU : [30, 50, 70], Survival loss scale : [50, 100, 150], Mini-batch size : [50, 75, 100], Learning rate : [1e-2], Hidden units in a cause-specific decoder module : [5, 10, 15], Number of layers in a cause-specific decoder module : [2,3]

Note that in training, we use **Survival loss scale** to put more focus on the log survival likelihood (i.e. $\log(L_{\text{surv}})$) than ELBO which captures data reconstruction loss.

Surv VAE-RNN Latent trajectory (Z^t) dimension : [32, 36, 40], Input embedding dimension : [40, 50, 60, 70], Hidden units in GRU : [30, 50, 70], Survival loss scale : [50, 100, 150], Mini-batch size : [50, 75, 100], Learning rate : [1e-2], Hidden units (Cause-specific decoder module) : [5, 10, 15], Number of layers (Cause-specific decoder module) : [2,3]

Dynamic-Deephit (Lee et al., 2020) Mini-batch size : [32, 64, 128], Dropout : [0.4, 0.6, 0.8], Learning rate : [1e-4, 1e-3, 1e-5], Hidden units (RNN) : [50, 100, 200, 300], Hidden units (Fully connected layer) : [50, 100, 200, 300], Number of layers (RNN) : [2, 4], Number of layers (Attention) : [2], Number of layers (Cause-specific module) : [1, 2, 3, 5], RNN type : [LSTM, GRU], Activation function (Fully connected layer) : [ReLU, Tanh, ELU], Activation function (RNN) : [ReLU, Tanh, ELU], β : [0.1, 0.5, 1]

RDSM (Nagpal et al., 2021a) Number of mixtures : [3, 4, 6, 8], Event time distribution : [LogNormal, Weibull], Learning rate : [1e-4, 1e-3], Hidden units (RNN) : [50, 100, 200], Number of layers (RNN) : [1, 2, 3, 5], RNN type: [LSTM, GRU, RNN]

Appendix C. Dana-Farber Cancer Institute (DFCI) data : cohort summary and additional performance results

C.1. Cohort summary

| | | Train | Valid | Test |
|----------------------|----------------------------------|--------|--------|--------|
| | n | 4797 | 1307 | 2630 |
| | Sex (female) | 0.537 | 0.526 | 0.554 |
| | Mean age | 60.467 | 60.775 | 60.574 |
| | Event rate (DVT) | 0.121 | 0.142 | 0.115 |
| | Event rate (all-cause mortality) | 0.463 | 0.481 | 0.464 |
| | Late stage/metastasis | 0.534 | 0.531 | 0.519 |
| Primary cancer sites | Gastrointestinal (GI) | 0.241 | 0.244 | 0.239 |
| | Lung | 0.167 | 0.179 | 0.164 |
| | Gynecologic (Gyn) | 0.097 | 0.093 | 0.097 |
| | Breast | 0.088 | 0.083 | 0.088 |
| | Genitourinary (GU) | 0.085 | 0.08 | 0.082 |
| | Unknown | 0.035 | 0.034 | 0.037 |
| | Thyroid | 0.025 | 0.026 | 0.02 |
| | Others | 0.263 | 0.26 | 0.273 |

Table 4: The DFCI data cohort summary in terms of number of patients, sex, age, event rates for DVT and all-cause mortality, late stage indicator, and diagnosed cancer types across train, validation, and test sets. Note that sex, late stage indicator, and diagnosed cancer types are shown in proportion.

| Cause of death | n | proportion |
|---|------|------------|
| Neoplasms | 3624 | 0.890 |
| Unknown | 145 | 0.036 |
| Diseases of the circulatory system | 85 | 0.021 |
| Diseases of the blood and blood-forming organs and certain disorders involving the immune mechanism | 56 | 0.014 |
| Diseases of the respiratory system | 39 | 0.010 |
| Certain infectious and parasitic diseases | 26 | 0.006 |
| Diseases of the digestive system | 16 | 0.004 |
| External causes of morbidity and mortality | 13 | 0.003 |
| Endocrine, nutritional and metabolic diseases | 12 | 0.003 |
| Diseases of the nervous system | 11 | 0.003 |
| Mental and behavioural disorders | 9 | 0.002 |
| Diseases of the genitourinary system | 8 | 0.002 |
| External causes of morbidity and mortality | 7 | 0.002 |
| External causes of morbidity and mortality | 6 | 0.001 |
| Certain infectious and parasitic diseases | 4 | 0.001 |
| Diseases of the musculoskeletal system and connective tissue | 3 | 0.001 |
| Symptoms, signs and abnormal clinical and laboratory findings, not elsewhere classified | 3 | 0.001 |
| External causes of morbidity and mortality | 3 | 0.001 |

Table 5: Summary table for causes of death among those who died ($n = 4,070$) in the in-house data. We obtained the death causes through National Death Index (NDI) data. We considered all-cause mortality as a competing event for time to DVT event prediction.

Shown in Table 4 is the DVT cohort summary in terms of number of samples, sex, age, event rates, late stage indicator, and diagnosed cancer types across train, validation, and test sets. And, shown in Table 5 is the summary of death causes obtained through National Death Index (NDI). We considered all-cause mortality as a competing event for time to DVT event prediction.

C.2. Additional performance results

| | Late stage/metastasis (n = 1366) | Lung (n = 432) | Gastrointestinal (GI) (n = 389) | Stomach/Pancreatic (n = 239) | Gynecologic (GYN) (n = 254) | Breast (n = 232) | Genitourinary (GU) (n = 216) |
|------------------------------------|-------------------------------------|----------------------|------------------------------------|---------------------------------|--------------------------------|----------------------|---------------------------------|
| SurvLatent ODE (Proposed model) | 0.733 (0.027) | 0.765 (0.038) | 0.630 (0.067) | 0.793 (0.037) | 0.580 (0.129) | 0.914 (0.055) | 0.874 (0.039) |
| Khorana scores (Imputed) | 0.634 (0.031)** | 0.615 (0.051)* | 0.632 (0.055) | 0.632 (0.070)* | 0.512 (0.131) | 0.688 (0.100)* | 0.554 (0.096)** |

Table 6: Performance summary of SurvLatent ODE and Khorana scores on various groups of patients defined by diagnosed cancer types and cancer stage for predicting DVT risk. As a performance metric, we utilized the mean of time-dependent AUC from 25th percentile to 75th percentile of DVT event times. Although model performances as well as performance differences vary widely across the groups, SurvLatent ODE outperforms imputed Khorana scores for all the groups except GI group. Standard errors, shown in parenthesis, as well as statistical significance (* : $p < 0.05$, ** : $p < 0.001$) were obtained exactly in the same manner as in the MIMIC-III experiment (see Table 1 caption).

C.3. Latent state explanation

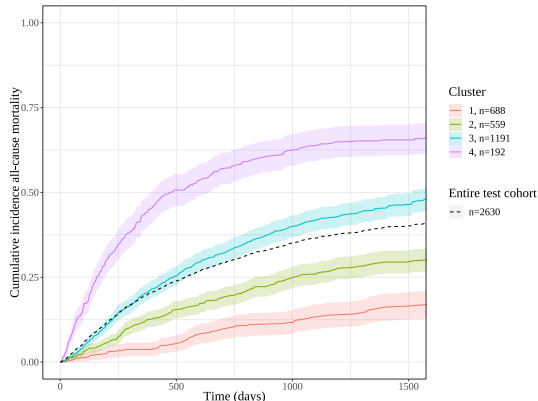


Figure 4: Cumulative Incidence trajectories, estimated by Aalen-Johansen Estimator for the all-cause mortality event across the clusters. The clusters were obtained, based on latent states output from the cause-specific decoder for all-cause mortality.

To obtain latent clusters, we utilized the temporal latent states output from the cause-specific decoder for DVT just before the fully-connected layer (see Fig. 1) at the inference time for the held-out test cohort ($n = 2630$). Then, we summed up the latent state of each patient across one year from their latest measurement (i.e. prediction time) and obtained the latent state matrix with dimension of $R^{N_{\text{test}} \times L}$, where L is the dimension of the latent trajectory. We then ran k-means clustering on the latent state using `sklearn` Python package (Pedregosa et al., 2011). Finally, we utilized the Aalen–Johansen estimator (Johansen, 1978) to non-parametrically estimate the survival trajectory of patients in each cluster. We used DVT-based latent clusters to obtain cumulative incidence trajectories for Fig. 3 and all-cause mortality based latent clusters (i.e. clusters based on latent states output from the cause-specific decoder for all-cause mortality) to obtain cumulative incidence trajectories for Fig. 4.

To interpret each cluster, we first obtained the baseline data for the test cohort at the prediction time using a forward-fill imputation method. Then, we used the standardized baseline data to run logistic regression ([Seabold and Perktold, 2010](#)) on each feature conditioning on Khorana scores and see how significantly the feature is associated with each cluster encoded as the binary label (i.e. one-versus-rest). Finally, upon investigating the significance of coefficients for each feature, we dropped a set of features without nominal significance ($p < 0.05$) for any of the clusters. The result is shown in the main text (Fig. 3).